Near-field Ion Energy and Species Measurements of a 5 kW Laboratory Hall Thruster

Frank S. Gulczinski III*, Richard R. Hofer*, and Alec D. Gallimore†
Plasmadynamics and Electric Propulsion Laboratory
Department of Aerospace Engineering
The University of Michigan
College of Engineering
Ann Arbor, MI 48109

ABSTRACT

The Plasmadynamics and Electric Propulsion Laboratory (PEPL) has used its Molecular Beam Mass Spectrometer (MBMS) to determine the ion energy distribution of the P5 5 kW laboratory Hall thruster. A skimmer was used to obtain a sample of the plasma in the near-field region, 10 cm downstream of the thruster exit plane. The thruster was operated at several discharge conditions and was rotated with respect to the sampling skimmer in order to determine ion energy profiles at various plume angles. These measurements were compared to far-field ion energy measurements taken 75 cm from the discharge plane in order to examine the evolution of the ion energy profile and the effects of testing environment on the results. Both ion energy measurements and time-of-flight mass spectroscopy revealed evidence of singly, doubly, triply, and quadruply charged xenon ions within the plume. Ion energy distributions were used to determine that the thruster's magnetic field was oriented such that the plume has an overall inward focus. It was seen that sampling the plasma closer to the thruster results in distributions that have undergone fewer changes as a result of collisions with other ions in the plume and with background neutrals within the test facility. Concerns regarding these facility effects have led to the development of a new Miniaturized Ion Energy Analyzer (MIEA) for future experimental work.

INTRODUCTION

Previous Hall thruster research has concentrated primarily on the 1.5 kW class of thrusters since they were of primary interest for commercial and military satellite use. However, driven by industry trends and IHPRPT (Integrated High Payoff Rocket Propulsion Technology) goals, the Hall thruster market is expanding beyond the 1.5 kW class thruster to both sub-kW thrusters for small satellites and high power thrusters for orbit transfer missions. Of particular interest for orbit transfer are thrusters of the 5 kW class. Several commercial thrusters are under development for this role. These include the SPT-140[1] and T-160[2] stationary plasma thrusters, the D-100[3] thruster with anode layer, and the Busek-Primex BPT-4000[4]. In order to keep its research as relevant as possible to future Hall thruster users, the University of Michigan, in conjunction with the United States Air Force, has developed a 5 kW class Hall thruster for basic research purposes.

This thruster, dubbed the P5 and shown in Figure 1, underwent performance and probe testing[5] that indicated it operated in a manner consistent with thrusters under commercial development.[6,7,8] Its purpose is to serve as a test bed for the development of diagnostics, investigations of Hall thruster physics, studies of spacecraft interaction issues, and development of next generation electric propulsion devices.[9,10,11,12]

---

* Graduate Student, Aerospace Engineering, Student Member AIAA
† Associate Professor, Aerospace Engineering and Applied Physics, Associate Fellow AIAA

Figure 1: University of Michigan/USAF P5 5 kW Hall Thruster

In this work, PEPL's Molecular Beam Mass Spectrometer (MBMS), initially developed by King,[13] was used to investigate the ion energy and charged species composition of the 5 kW Hall thruster. The purpose of this work was threefold. First, the test facility had undergone a pumping upgrade since King's tests (see next section) which lowered the pressure during testing, thereby reducing the chance of plume ions colliding with background neutral particles. By reducing the collision probability we obtain measurements that are more representative of the true plasma distributions. Second, flexibility in choosing the operating conditions of this Hall thruster allowed for testing at multiple operating points. This is important since many operational concepts require the Hall thruster to perform several missions at different power levels over the lifetime of the satellite. Third and most importantly, the system was modified to allow near-field measurements to be taken by placing a sampling orifice 10 cm away from the discharge plane of the thruster. This allowed for an investigation of the evolution of ion energy and charge state profiles, as well as facility effects.

EXPERIMENTAL SETUP

Tests were performed in PEPL's 6 m by 9 m Large Vacuum Test Facility (LVTF). This is the same facility used in previous work at PEPL[14], but prior to these tests, it was refitted with four CVI model TM-1200 Re-Entrant Cryopumps. Each cryopump is surrounded by a liquid nitrogen baffle, as shown in Figure 2. These cryopumps have replaced the diffusion pumps previously used for high vacuum work. They provide a xenon pumping speed measured at 140,000 l/s with a base pressure of $2*10^{-7}$ Torr. Pressure was determined by averaging the measurements of two ion gauges: a Varian model 571 gauge with a HPS model 919 Hot Cathode Controller and a Varian model UHV-24 nude gauge with a Varian UHV senTorr Vacuum Gauge Controller. The Varian nude gauge, the senTorr controller, and the connecting cable were calibrated as a unit on nitrogen. A calibration factor of 2.87 was used to correct for xenon.[15] Propellant flow was controlled by two MKS model 1100 Flow Controllers, which were calibrated using a known volume and the ideal gas law corrected for the compressibility of xenon.

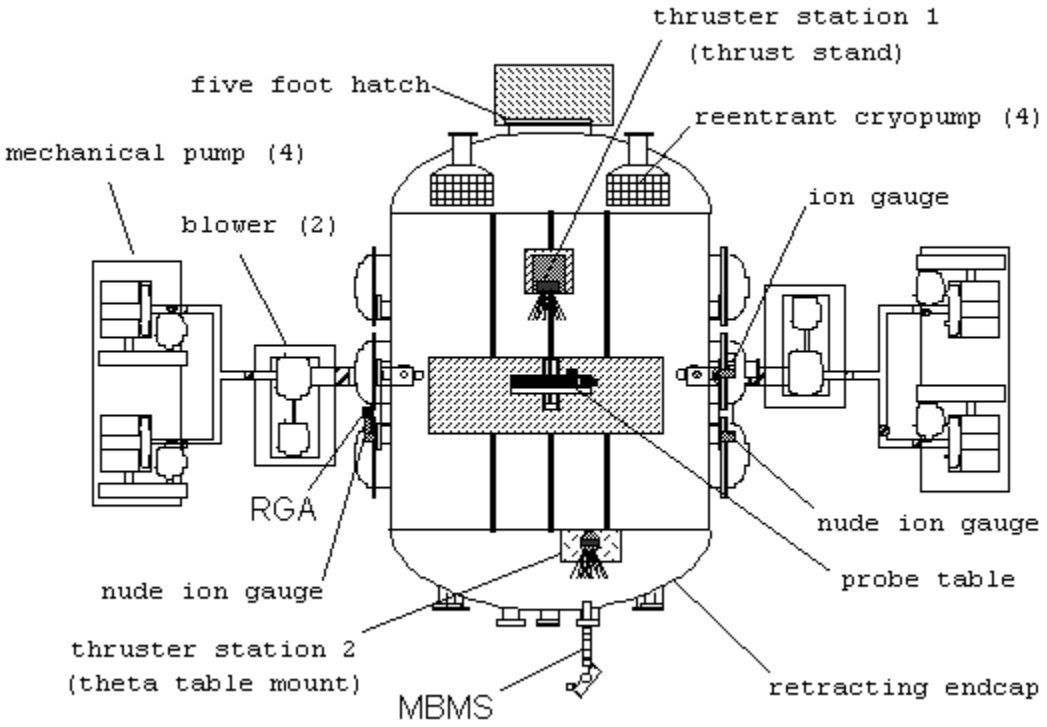

Figure 2: University of Michigan Large Vacuum Test Facility

Laboratory power supplies were used to provide thruster power. The main discharge was supplied by a Sorensen model DCR 600-16T. Current was supplied to the inner and outer electromagnets by a Kikusui model PAD 55-10L and a Kikusui model PAD 35-10L, respectively. The cathode heater and igniter were powered by a Kepco model ATE 36-30M and a custom-built high voltage ignition supply. The discharge circuit of the thruster was electrically isolated during operations. A filter consisting of 1.3 Ω equivalent resistance in series with the discharge current and a 95 μF capacitor in parallel was used to dampen thruster oscillations.

The MBMS is a time-of-flight mass spectrometer with a 45-degree parallel plate energy analyzer. It is essentially two instruments in one, that when used together can give direct measurements of both ion energy and species composition. The mass spectrometer is mounted to one end of the LVTF. Ions pass into the MBMS through a sampling orifice. Two diffusion pumps are used to evacuate the MBMS in order to reduce the chance for collisions between beam ions and background gas. The beam enters the 45-degree energy analyzer, which allows only ions of a specific energy-to-charge ratio to pass through and reach the detector. This ratio is selected by setting the electric field between the plates of the analyzer. By sweeping the value of this field, an entire ion energy distribution function can be determined.

For species composition, the time-of-flight mass spectrometer is used. This is the same physical system, with an electrostatic beam gate placed just downstream of the sampling orifice. By pulsing the gate open and recording the time it takes for the ions to reach the detector at the end of the energy analyzer, the individual species of the plasma can be detected. This can be done because, while all of the ions passing through the analyzer for a given pass voltage have the same energy-to-charge ratio, the Hall thruster accelerates them to different velocities based on their charge state. Since their velocities are different, they will arrive at the detector at different times. Reference 13 provides more detail regarding the theory and development of the 45-degree energy analyzer and the time-of-flight system.

The thruster was mounted at Thruster Station 2, as seen in Figure 2, on a New England Affiliated Technologies (NEAT) rotary positioning table. This allows it to be rotated with respect to the sampling orifice. This table has an angular accuracy of 0.05° and a repeatability of 0.007°.

For measurements 75 cm from the thruster exit plane, the system was configured as shown in Figure 3. For these measurements, the center of rotation was the center of the thruster. Ion energy measurements were taken in 5° increments from 0° until loss of signal – typically ~105°. Because the signal intensity drops off rapidly away from centerline, species composition measurements were taken at 0° only. The sampling orifice was aligned with the 45-degree energy analyzer entrance slit by passing a laser through the entrance slit such that it was parallel to the ion beam path. The sampling orifice was then aligned to that beam. The thruster angle was set such that the laser was tangent to the face of the thruster when it was oriented at 90°. For ion energy measurements, the 45-degree pass voltage was swept from 0 to 1000 V in 1 V increments by a Keithley model 2410 SourceMeter. This sourcemeter had a rated accuracy of better than 0.012% over the full rage of interest. Due to the nature of the energy analyzer,[13] this results in a sweep of ion energy of 0 to 1800 V. For species composition, measurements were taken at the peak ion energy, as determined using the 45-degree energy analyzer, and in 20 V increments above and below that voltage. The time-of-flight path length was 2.34 m.

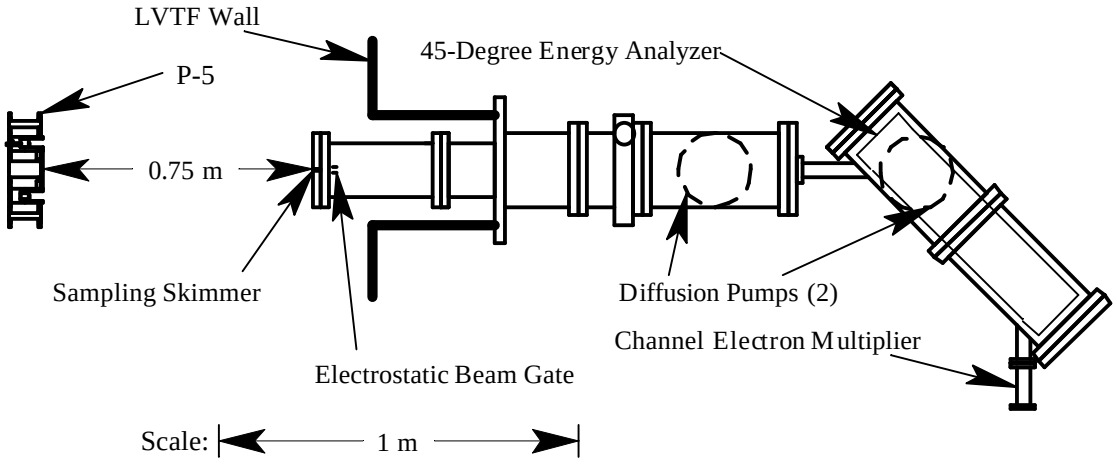

Figure 3: Far-field Configuration

For near-field measurements, 10 cm from the thruster exit plane, an extension to the system was built. The extension is shown with the complete system in Figure 4 and in detail in Figure 5. This added approximately 67 cm of length to the system. For these measurements the center of rotation was the center of the annular discharge chamber. This was done so that the ion energy contributions of one side of the discharge chamber could be examined independently of the other so as to minimize the detection of crossover flow. Ion energy measurements were taken in 5° increments from 0° until loss of signal – typically ~90°. Again, species composition measurements were taken at 0° only. Alignment was performed in the same manner as for the far-field measurements. Ion energy and species composition measurements were performed over the same range as for far-field measurements. For the near-field measurements, the time-of-flight distance was increased to 2.92 m due to the use of a miniaturized gate near the sampling skimmer.

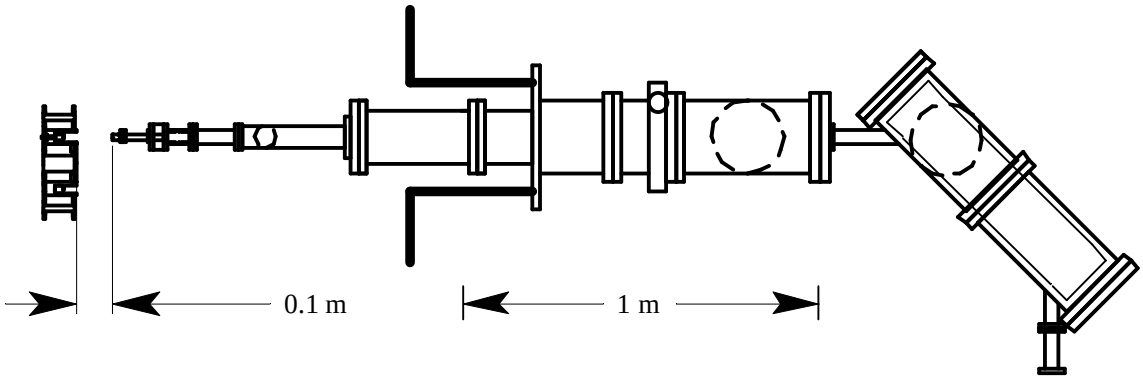

Figure 4: Near-field Configuration

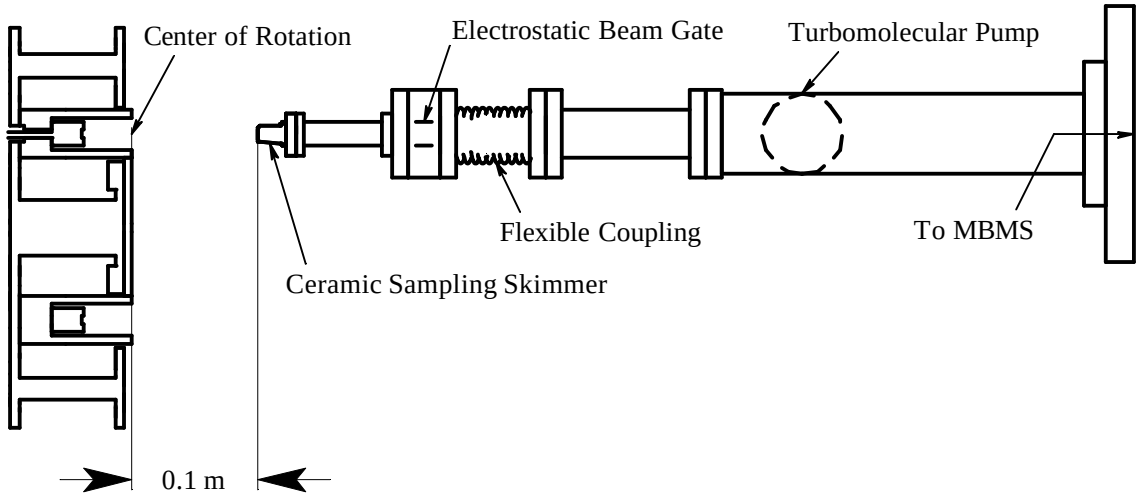

Figure 5: Near-field Sampling Skimmer

EXPERIMENTAL RESULTS

For both the near and far field, attempts to take data at three thruster operating conditions were made. These conditions are summarized in Table 1. Also listed are the tank pressures during these tests, corrected for xenon and averaged between two ion gauges. For comparison, during King's tests on the SPT-100 the maximum chamber pressure was $5*10^{-5}$ Torr. Condition 1 represents running the thruster in a mode similar to a 1.5 kW Hall thruster such as the SPT-100 or D-55 TAL. Condition 3 is the full power 5 kW case. Condition 2 is an intermediate case that shares a current with Condition 1 and a voltage with Condition 3, allowing for comparisons while changing only one variable. Successful ion energy measurements were taken at all three conditions for both the near and far field. Complete species composition traces were taken at Condition 1 and Condition 2 in the far field. For far-field species measurements at Condition 3, an experimental failure interrupted the test. As will be shown later, based on the data that was collected it was decided that the experiment did not require completion. Species composition traces were also taken at Condition 1 and Condition 2 in the near field. Measurements were not taken for Condition 3 because operating the thruster at the high anode mass flow rates needed for a 10 A discharge in close proximity to the sampling skimmer resulted in neutralized propellant backstreaming into the discharge chamber. When this occurred, the thruster responded as if the anode mass flow rate had been increased - with an increase in current. Thus, the thruster was being forced to operate at an off-nominal condition. This was not a problem during the ion energy measurements because they took far less time to complete.

	Discharge Voltage [V]	Discharge Current [A]	Total Flow Rate [sccm]	Tank Pressure [Torr]
Condition 1	300	5.3	64	$5.5*10^{-6}$
Condition 2	500	5.3	64	$5.5*10^{-6}$
Condition 3	500	10.0	111	$8.5*10^{-6}$

Table 1: Thruster Operating Conditions – Cathode Flow Rate = 6 sccm for All Cases

When examining the ion energy results, we expect to see the results of two types of collisions: elastic collisions between ionic species, and inelastic charge exchange collisions between ionic species or between ions and neutral particles. These collisions can be recognized based on the following characteristics:

Elastic Collisions (between an ion of charge q=1 and an ion of charge q=n):

- A high voltage "tail" on the singly charged ion voltage/charge distribution that decays to zero at a voltage/charge equal to n times the maximum voltage/charge of the ion with charge n (in its pre-collision distribution)
- A low voltage "tail" on the voltage/charge distribution of the ion with charge n that decays to zero at a voltage/charge equal to 1/n times the minimum voltage/charge of the singly charged ion
- These "tails" decay monotonically without any local maxima

Since these ions see the same accelerating voltage, the maximum voltage/charge will be the same and will be very close to, but less than, the thruster discharge voltage. Thus, for n=2, the high voltage "tail" will decay to zero at approximately twice the discharge voltage. The minimum voltage/charge is more difficult to define as it depends on how far the accelerating potential drops within the ionization zone of the thruster. The peaks of both voltage distributions will occur at the same value of voltage/charge.

Charge Exchange (CEX) Collisions

- CEX collisions produce appendages to the main distribution that do not decay monotonically as in the case of elastic collisions
- These appendages exhibit local maxima corresponding to the energy distribution of the colliding species
- CEX collisions conserve the shape of the original distribution
- Ion-Neutral CEX collisions only produce detectable ions at voltage/charge ratios greater than the original ion, whereas Ion-Ion CEX collisions can produce detectable ions at voltage/charge ratios above and below the original ions (neutral particles produced in these collisions are not detectable by the MBMS)

For example, if a doubly charged ion, accelerated by a potential V (thus energy, E~2V, since E=qeV), undergoes a CEX collision with a neutral atom (with zero velocity), there are two possible outcomes. In the first, there could be two electrons transferred from the neutral atom to the ion. However, this would result in a doubly charged ion with zero velocity – which will not travel to the detector, and a neutral atom with E~2V – but since neutrals do not pass through the 45-degree energy analyzer, it will not be detected. Thus the first outcome cannot be observed. The second outcome, however, can be observed. If one electron is transferred to the doubly charged ion, the resulting singly charged ion would have twice the energy of a normally produced singly charged ion. Thus, in the voltage/charge domain of the measurements of the MBMS, it will appear as a maximum at twice the most probable voltage found in the main distribution.

Ion Energy

Figures 6 through 8 show the far-field ion energy distributions for all three thruster operational conditions at an angle of 0 degrees (thruster pointed directly toward the sampling orifice).

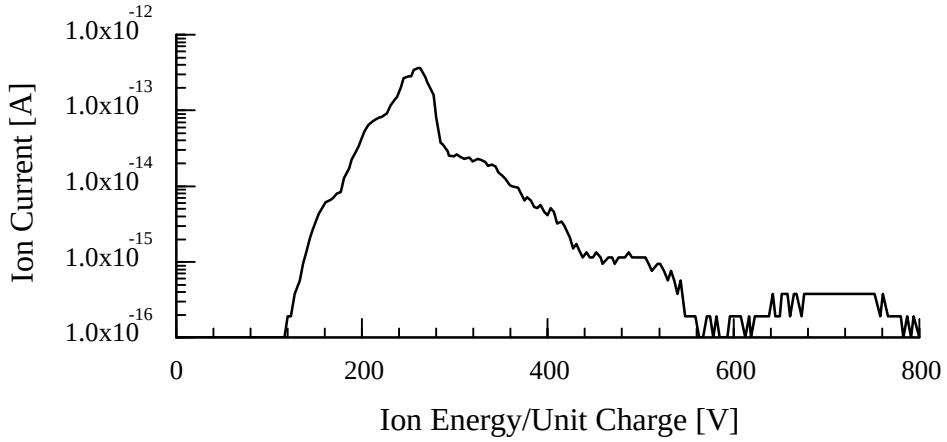

Figure 6: Far-field Ion Energy Distribution - 0 Degrees - Condition 1 [Semi-log plot]

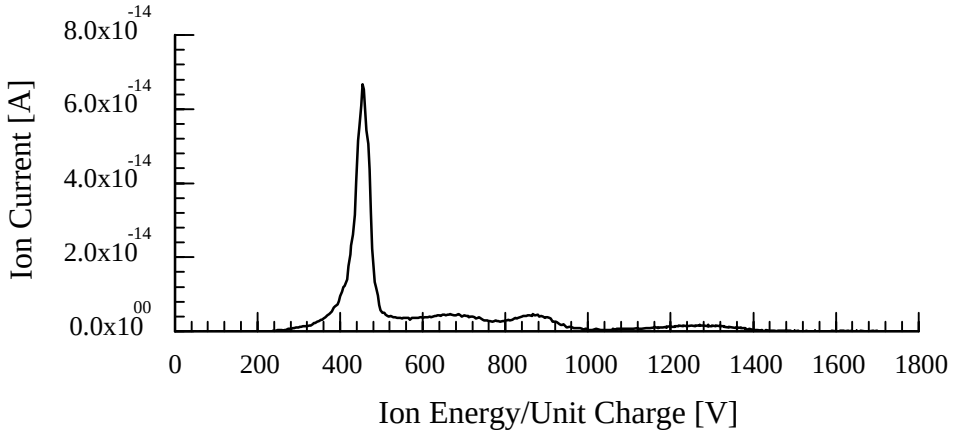

Figure 7: Far-field Ion Energy Distribution - 0 Degrees - Condition 2

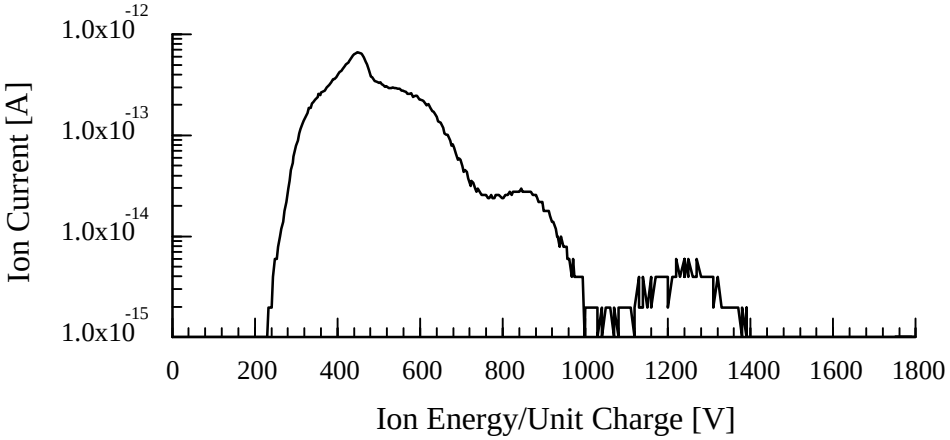

Figure 8: Far-field Ion Energy Distribution - 0 Degrees - Condition 3 [Semi-log plot]

In Figure 6, for Condition 1, the primary ion energy distribution has its peak at 263 V with respect to ground. For this condition, the plasma potential was approximately 7 to 8 V above ground. The peak is approximately 90% of the discharge voltage, which is what is expected for a well-developed Hall thruster.[16] In this distribution, we see strong evidence of elastic collisions between singly and doubly charged xenon ions, decaying at twice the discharge voltage. This behavior is very similar to that observed by King for the SPT-100. When this distribution is examined more closely on a semi-log plot as shown, small CEX collision peaks at 2X and 3X the primary peak are seen. Since there are no CEX peaks at voltages less than the primary peak, it appears that these peaks are the result of collisions by neutrals with doubly and triply ionized xenon that resulted in singly charged ions.

In Figure 7, for Condition 2, the primary distribution has its peak at 454 V with respect to ground and the plasma potential was approximately 7 to 8 V above ground. Again, as expected, the peak is approximately 90% of the discharge voltage. In this distribution, there is some indication of elastic collisions. There are, however, very noticeable ion-neutral CEX collision peaks at 1.5X, 2X, and 3X the primary peak. The 2X and 3X peaks are the result of collisions by neutrals with doubly and triply ionized xenon that resulted in singly charged ions. The 1.5X peak results from a collision of triply ionized xenon with a neutral that produced a doubly charged ion.

In the case of Condition 3 (Figure 8), the total flow rate has almost doubled, going from 64 sccm to 111 sccm. The peak of the primary distribution is 449 V with respect to ground and the plasma potential is 10 V above ground. As will be discussed later, the increase in flow rate leads to a large pressure build-up in front of the entrance orifice to the MBMS that increases the collision probability considerably. This is reflected in the ion energy distribution that shows significant elastic collision broadening. The 2X and 3X peaks similar to those observed for Condition 2 are evident in the semi-log plot, but any chance of observing the 1.5X peak is obscured by the broadening.

As the thruster is rotated to higher angles, similar trends were seen for all three conditions. For Condition 1, the profile changes very little from 0 to 40 degrees, maintaining the same shape as seen in Figure 6. Then, as shown in Figure 9, at 45° the profile begins to broaden significantly toward the lower energy side of the distribution. This trend continues to approximately 50° and then transitions into a shift of the primary peak location as seen at 60° where the maximum of the primary peak is at 205 V. At angles where this broadening and shift are seen, the ion current intensity is significantly lower than in areas where the distribution has its peak at the same voltage as at 0°. Beginning at 65°, the profile shifts back to the same shape seen at centerline. The intensity of the signal also increases, though it is far less than at centerline. The next region begins at approximately 85°, where we see evidence of significant numbers of ion-ion CEX collisions and a highly attenuated peak at the centerline voltage. The last signal region occurs at 100°, where we see a low intensity distribution of low energy ions created outside the discharge chamber. Beyond this, the signal fades into the noise at 105°.

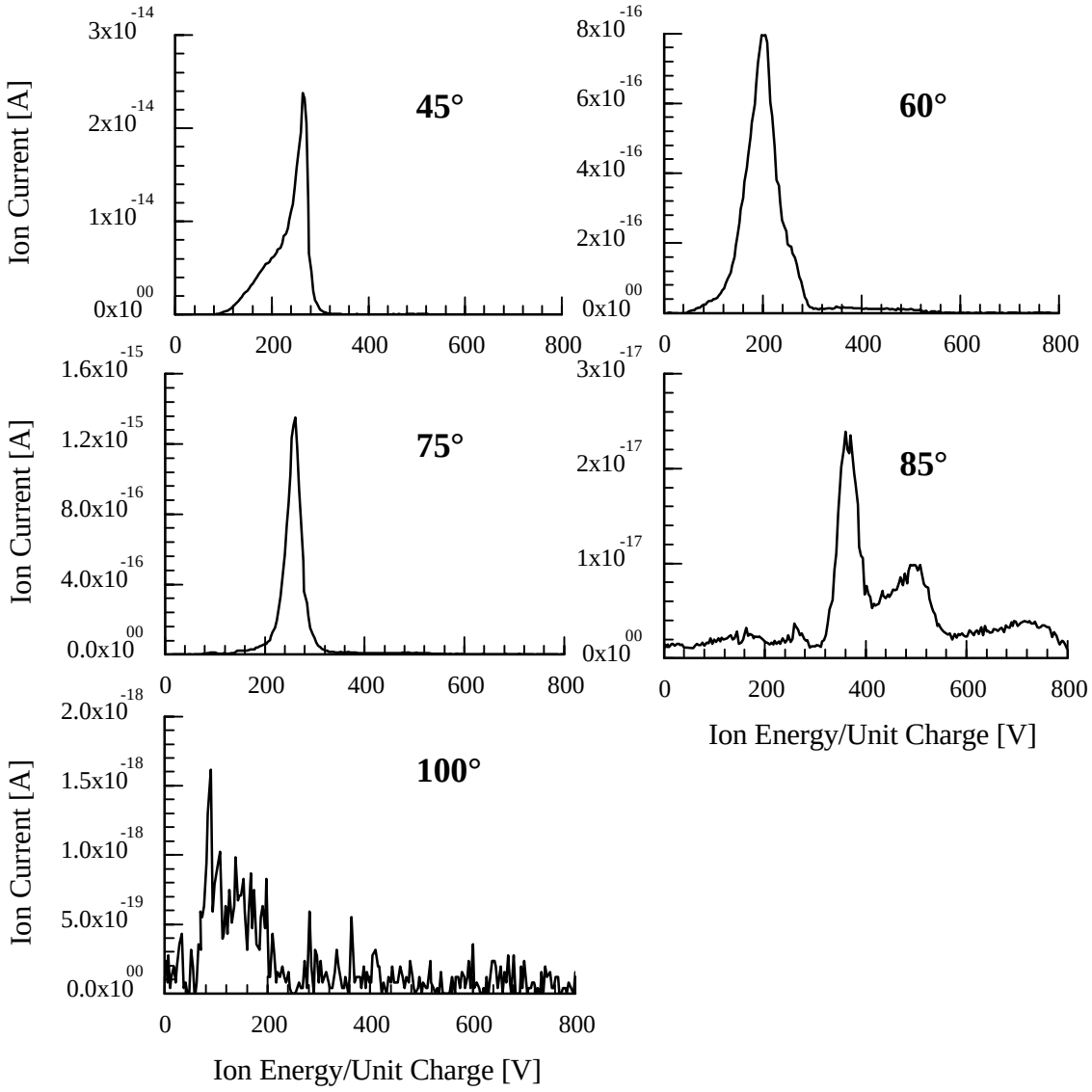

Figure 9: Off-Centerline Far-field Ion Energy Distributions - Condition 1

For Condition 2, the distributions retain the centerline shape of Figure 7 out only to 10°. Behavior at higher angles is illustrated in Figure 10. From 15° to 30°, the low energy side of the distribution grows, and is accompanied by high energy CEX collision peaks at 2X and 3X the peak voltage. This then transitions into a peak shift, though it is slightly different than for Condition 1. From 35° to 50°, the primary peak remains and is approximately the same intensity as the shifted peak. At these angles there is also a significant 2X CEX peak. Then, from 60° to 70°, the primary peak regains dominance, though the shifted peak remains – in this range, there is no 2X CEX collision peak. The signal then shifts back toward the centerline shape before becoming dominated by high energy ion-ion CEX peaks at 85°. Again there is a low energy distribution at 100° and the signal fades into the noise at 105°.

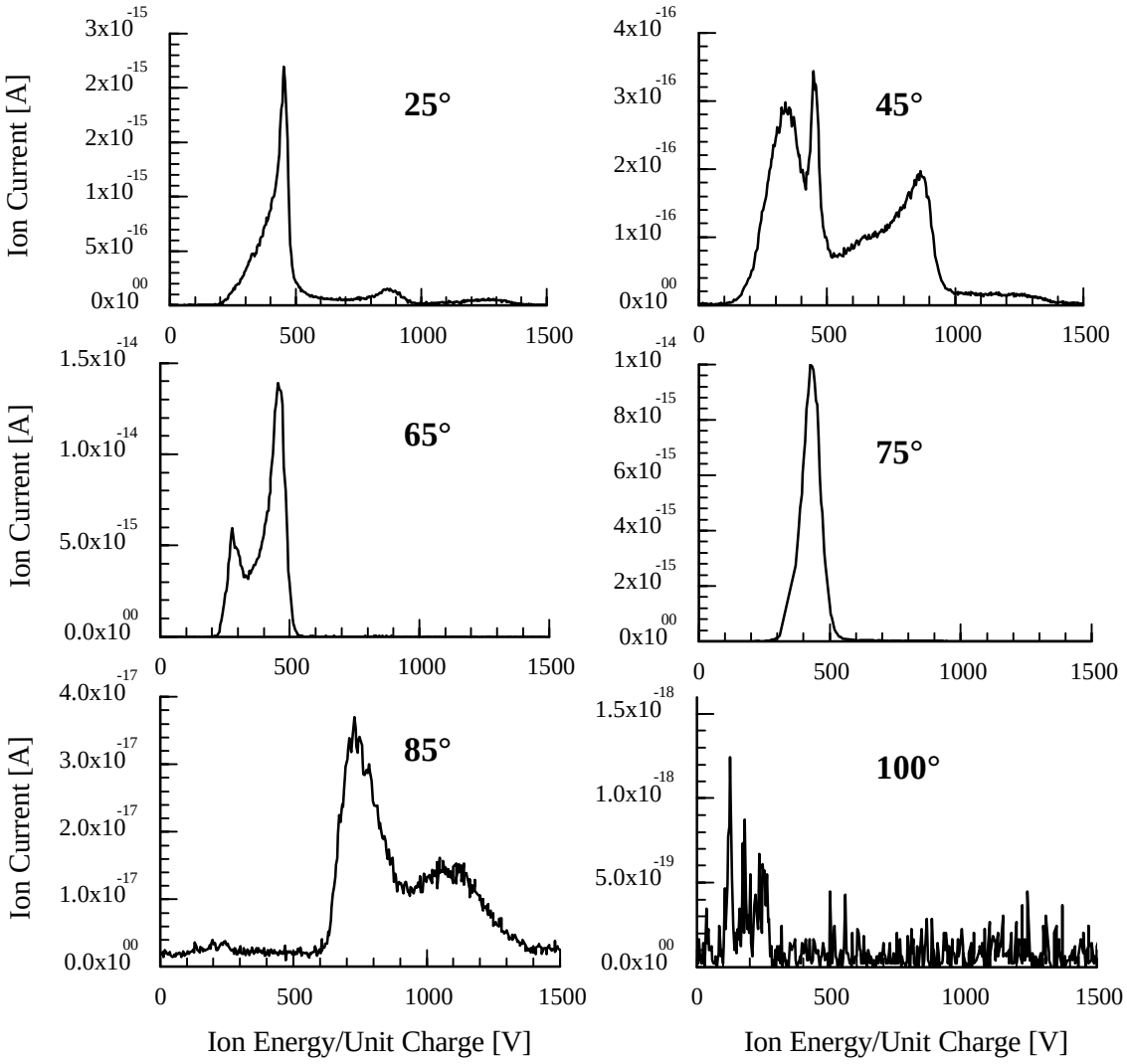

Figure 10: Off-Centerline Far-field Ion Energy Distributions - Condition 2

For Condition 3, the trends are qualitatively similar with subtle dissimilarities and are presented in Figure 11. The collision broadened centerline shape seen in Figure 8 remains out to 35°, with the broadening decreasing with angle, before increasing at 40°. Then from 45° to 60°, we see the peak shift. The peak then shifts back to the centerline voltage at 65°. It remains there until 80°, then begins to decrease in voltage, falling to 394 V at 95°. However, this peak shift is different than that typically seen around 45° because it is not accompanied by the broadening that characterizes the lower angle shift. The signal fades into noise at 100°, without experiencing the CEX collision or low ion energy regions.

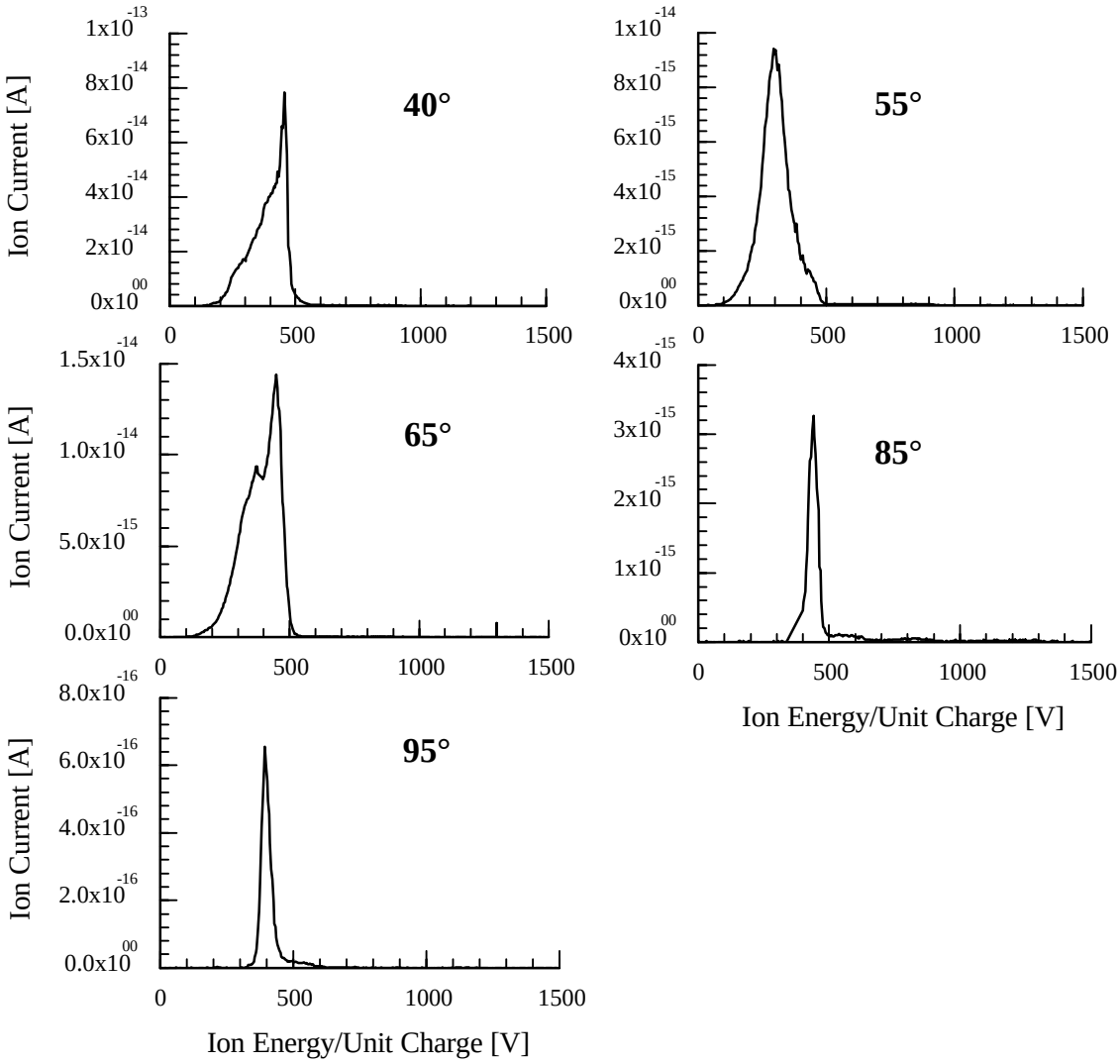

Figure 11: Off-Centerline Far-field Ion Energy Distributions - Condition 3

We now proceed to examine the near-field ion energy distributions, again starting with the 0° distributions for all three conditions.

In Figure 12, for Condition 1, the primary peak again has its maximum at 263 V. In the near field, the profile is CEX collision dominated. Upon closer examination, we see peaks at 1.33X, 2X, and 3X the discharge voltage. A peak at 1.33X indicates a CEX collision between a quadruply charged xenon ion and a neutral xenon atom with one electron exchanged. Peaks at 1.5X for triply charged xenon becoming doubly charged and at 4X for quadruply charged xenon are not seen at 0°, but are seen from 5° to 15° (see Figure 15).

In Figure 13 at Condition 2, the primary peak has a maximum at 456 V. Close examination shows that the profiles are again dominated by CEX collisions. Peaks are observed at 1.33X, 1.5X, 2X, and 3X the primary peak (due to their proximity, the 1.33X and 1.5X peaks tend to blend together into a single "bump" with two maxima). For most of the sweeps at Conditions 2 and 3, we observe an increase in intensity at the end of the scanning range. It is hypothesized that this is the beginning of the peak at 4X the primary peak (~1800 V). Unfortunately, the scanning range of the sourcemeter is not sufficient to encompass this peak in its entirety.

The results for Condition 3 (Figure 14) are very similar to Condition 2, and do not suffer the broadening seen for the far-field measurements. It was, however, very difficult to take measurements at this condition, and many sweeps showed unusual amounts of noise and other detrimental effects.

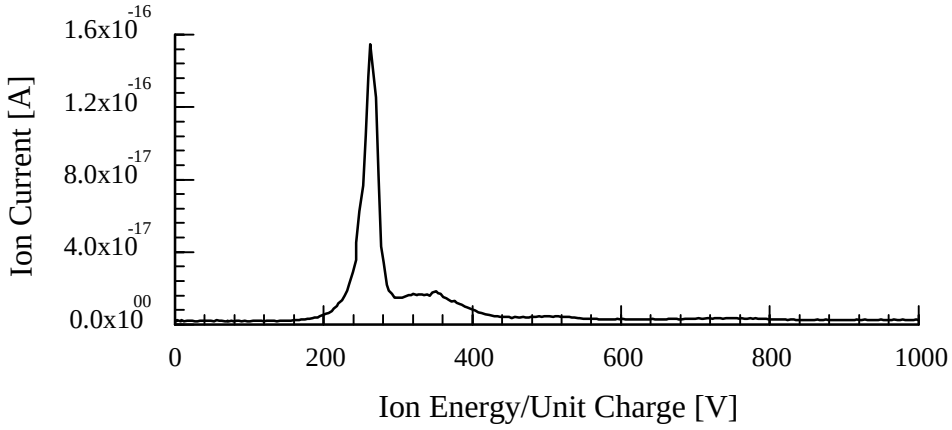

Figure 12: Near-field Ion Energy Distribution - 0 Degrees - Condition 1

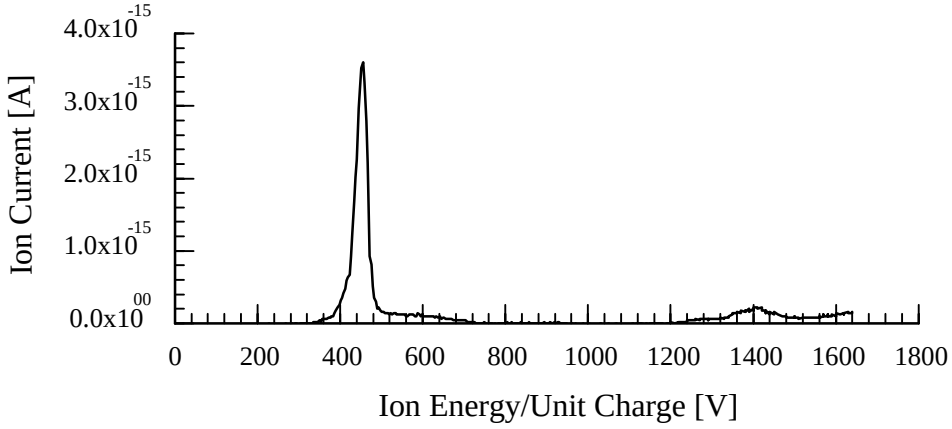

Figure 13: Near-field Ion Energy Distribution - 0 Degrees - Condition 2

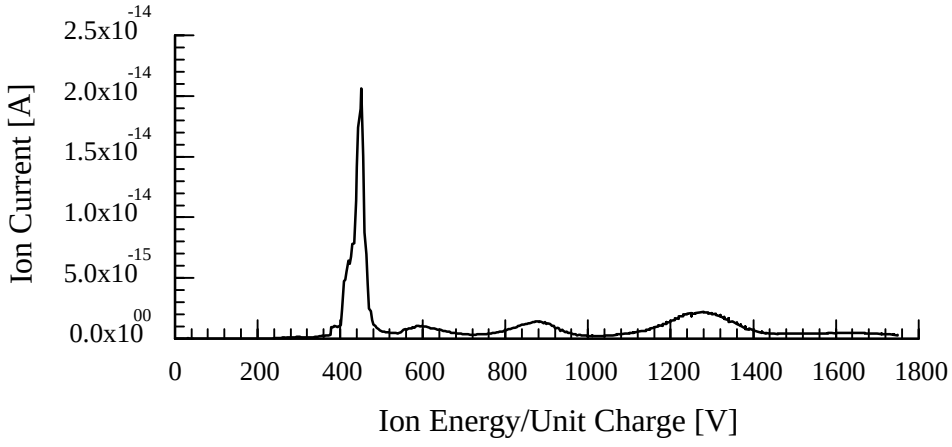

Figure 14: Near-field Ion Energy Distribution - 0 Degrees - Condition 3

As was seen for far-field measurements, when the thruster is rotated to higher angles, similar trends are observed for all three conditions. They are illustrated in Figure 15 for Condition 1. The centerline profile, seen in Figure 12 is maintained to 40° off centerline. Then from 45° to 55°, there are strong 2X and 3X CEX peaks. From 60° to 85°, the CEX peaks remain, but the primary peak at 263 V is attenuated as seen at 70°. The primary peak briefly regains dominance at 90°, before the signal fades into the noise at 95°.

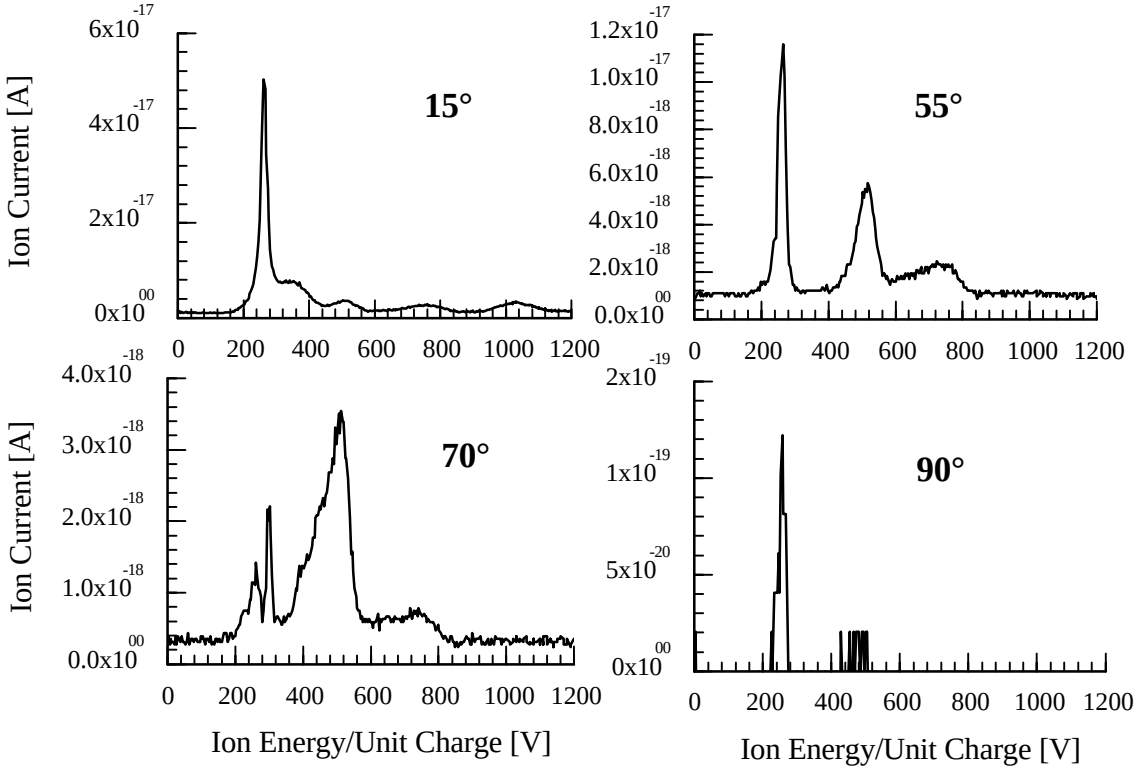

Figure 15: Off-Centerline Near-field Ion Energy Distributions - Condition 1

For Condition 2, the trends are almost identical. The only differences were that the primary peak at 456 V did not attenuate until an angle of 65°, instead of 60°, and the signal fades into the noise at 90°, before the primary peak has an opportunity to reappear.

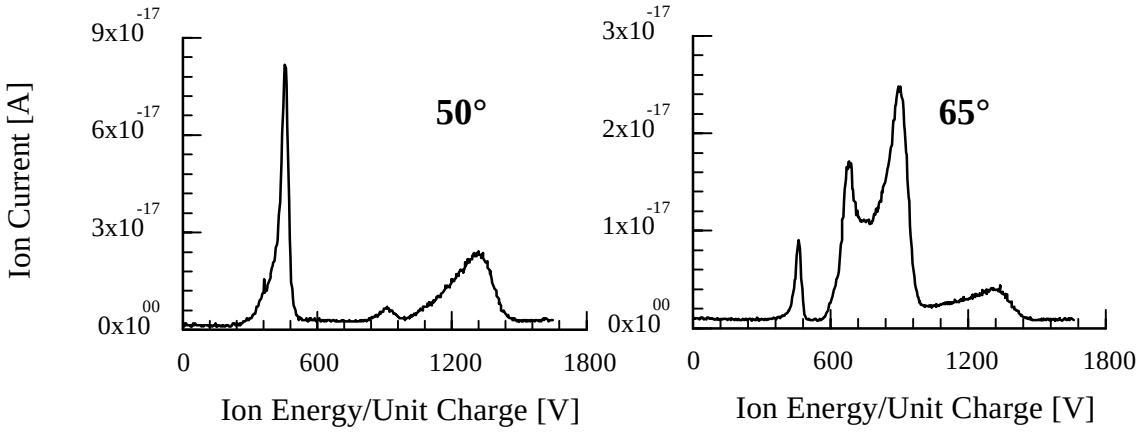

Figure 16: Off-Centerline Near-field Ion Energy Distributions - Condition 2

Once again, Condition 3 (Figure 17) is somewhat different. The centerline structure remains to an angle of 15° with a maximum at 451 V. We then see significant CEX collision peaks from 20° to 40°. From 45° to 80°, these peaks fade, and the signal returns to a profile similar to centerline, though with significant collisional broadening on the low energy side. At 85°, the peak voltage begins to shift downward, similar to the far-field case, reaching 405 V at 90° before the signal fades into noise at 95°.

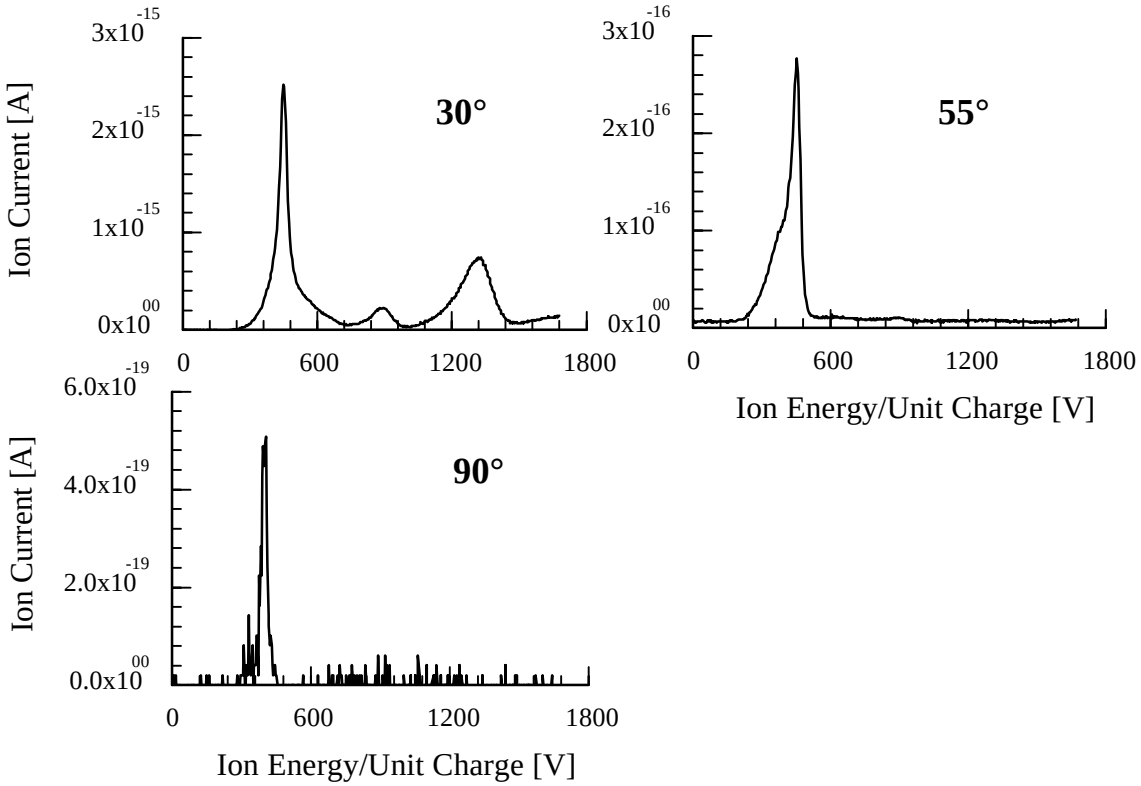

Figure 17: Off-Centerline Near-field Ion Energy Distributions - Condition 3

Time-of-flight Mass Spectroscopy

Next we examine the results for species measurements obtained using the time-of-flight configuration of the instrument.

Beginning again with the far field, we look at the traces obtained as the ion beam is gated, allowing ions to separate based on their charge state. The peaks are measured on an oscilloscope versus time, then converted to a horizontal scale in terms of mass/charge. This is done using the time-of-flight distance and the pass voltage of the 45-degree energy analyzer (which is proportional to the acceleration potential that the ions experience and thus their velocity). The following profile was taken at 0° for Condition 1 at the primary peak (263 V).

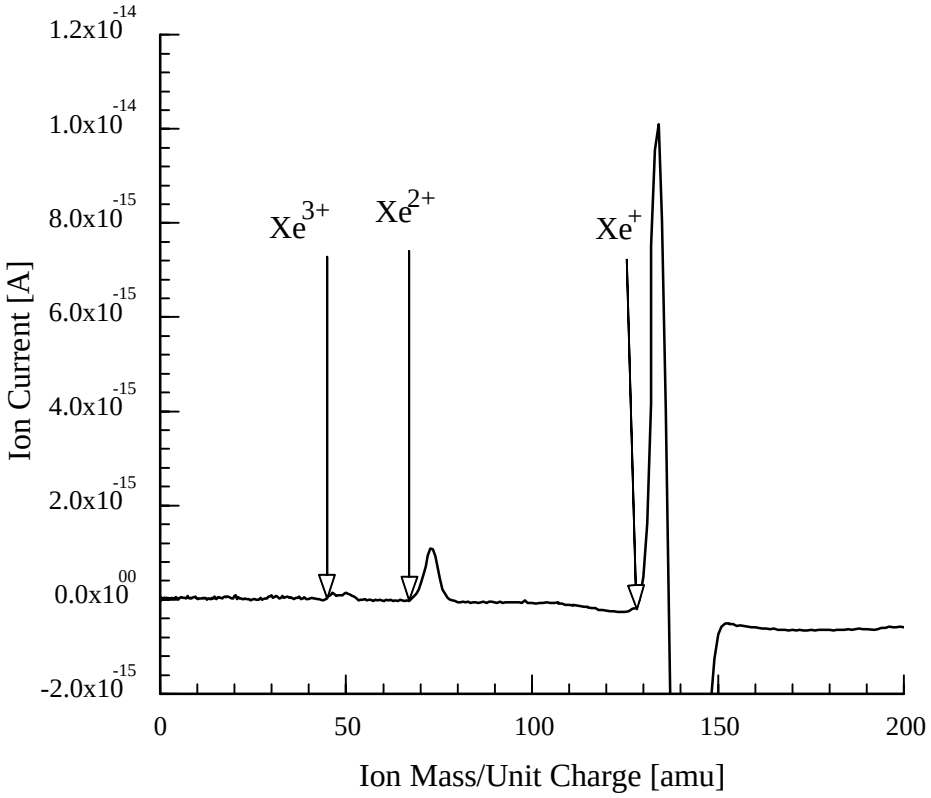

Figure 18: Far-field Time-of-flight Peaks for Condition 1 - Primary Voltage (263 V)

In this trace, singly, doubly, and triply ionized xenon were observed at 131, 65.5, and 44 AMU, respectively. The point of arrival of a species corresponds to the beginning of the rise of a peak. The width of the peak relates to the length of time that the gate is left open. If the gate is left open for a sufficient amount of time such that the peak is not clipped by the closing of the gate, the intensity is related to the density of a particular species. For a particular accelerating potentials, the individual species fraction, f_i, can be determined using the following equation, where I_i is the signal intensity and q_i is the charge.

$$f_i(V) = \frac{I_i / \sqrt{q_i}}{\sum_i \left(I_i / \sqrt{q_i} \right)}$$

The fractions were determined at various accelerating potentials for all three conditions and are given in the following figures, along with a normalized ion energy trace taken at 0 degrees for reference. They show local maxima of double and triple ion fraction that correspond closely to bumps in the ion energy distribution, thus confirming their role as collisional products

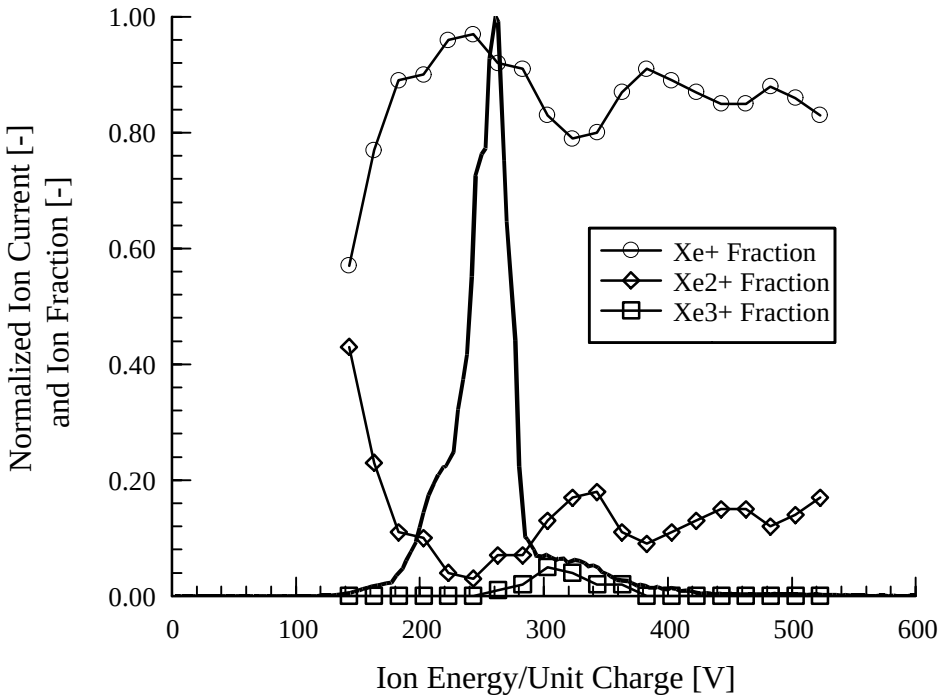

Figure 19: Far-field Ion Fractions at Condition 1 - 0 Degrees

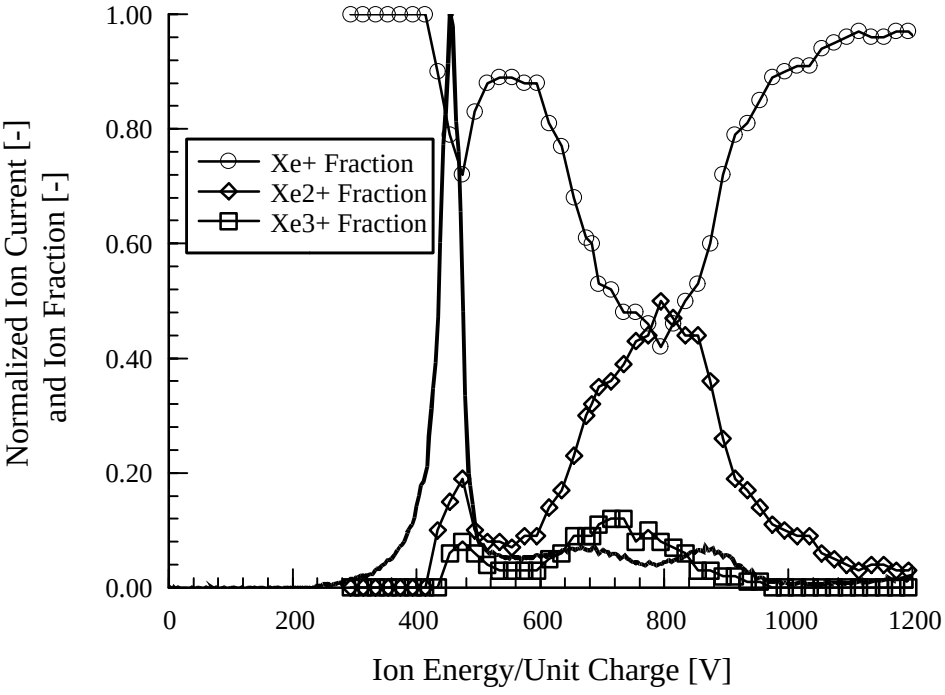

Figure 20: Far-field Ion Fractions at Condition 2 - 0 Degrees

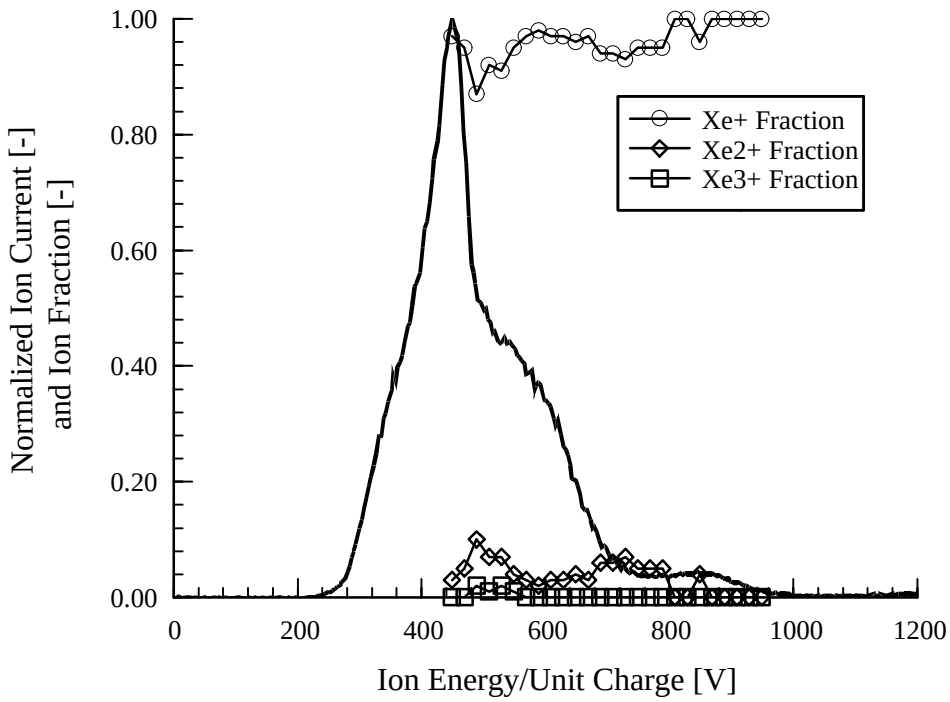

Figure 21: Far-field Ion Fractions at Condition 3 - 0 Degrees

The readings taken at Condition 3 were cut short by an experimental failure. Examining Figure 21, we see that the species fractions are dominated by singly ionized xenon. It is believed that the large anode mass flow rate required for operating the thruster at 10 A results in a highly collisional zone in front of the sampling orifice. Previous measurements of Hall thruster plumes have shown that approximately 90% of the plume is singly ionized xenon.[13,17] In a high collision area, beam ions will undergo ion-neutral CEX collisions that lower the plasma's overall total charge state. Collisions between neutrals and double or triple ions will depopulate these charge states in favor of singly ionized xenon. However, when singly ionized xenon undergoes a collision, it is neutralized and removed from the total beam ion population. Therefore, collisions reduce the total number of beam ions but increase the fraction of singly charged ions. This has shown that under high flow rate conditions, facility effects can artificially reduce species fractions. For this reason, along with the large amount of sputtering that occurs when the thruster is operated at 10 A, these tests were not continued.

For near-field measurements, we again present a trace of the species peaks versus mass for Condition 1 at the maximum of the ion energy distribution (263 V) in Figure 22. Longer gate times were necessary for these measurements to obtain a clear, non-clipped signal. The gate time is short enough, however, to allow for species differentiation. In addition to the singly, doubly, and triply ionized xenon that was detected in the far field, we detect the presence of a peak at 32 AMU. This could correspond to two different species: quadruply ionized xenon or ionized oxygen molecules. However, in our near-field ion energy measurements we detected CEX peaks at 1.33X and 4X the primary discharge peak, which correspond to quadruply ionized xenon. Additionally, O_2^+ is expected to be very uncommon since it would have to survive being ingested, ionized, and accelerated by the thruster without dissociating. Thus, there are two measurements that act as independent confirmation of the presence of Xe^{4+} in the plume. Collisions that remove quadruply ionized xenon from the system are greater in number than those that produce it. Therefore, by the time a sample is taken 75 cm from the thruster, almost all of the quadruply charged xenon has been converted to a lower charge state ion or neutral, increasing the fraction of these other ions in the process.

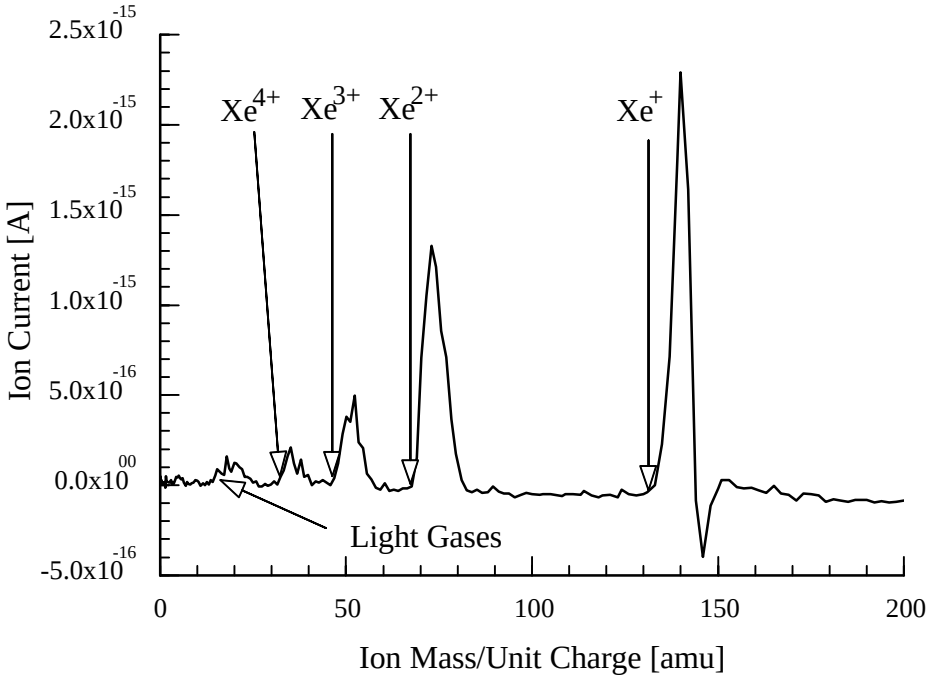

Figure 22: Near-field Time-of-flight Peaks for Condition 1 - Primary Voltage (263 V)

Figure 23 and Figure 24 provide the near-field ion fractions for a range of acceleration voltages at Condition 1 and Condition 2, respectively. Again peaks in the multiply charged species closely correspond to ion collision peaks.

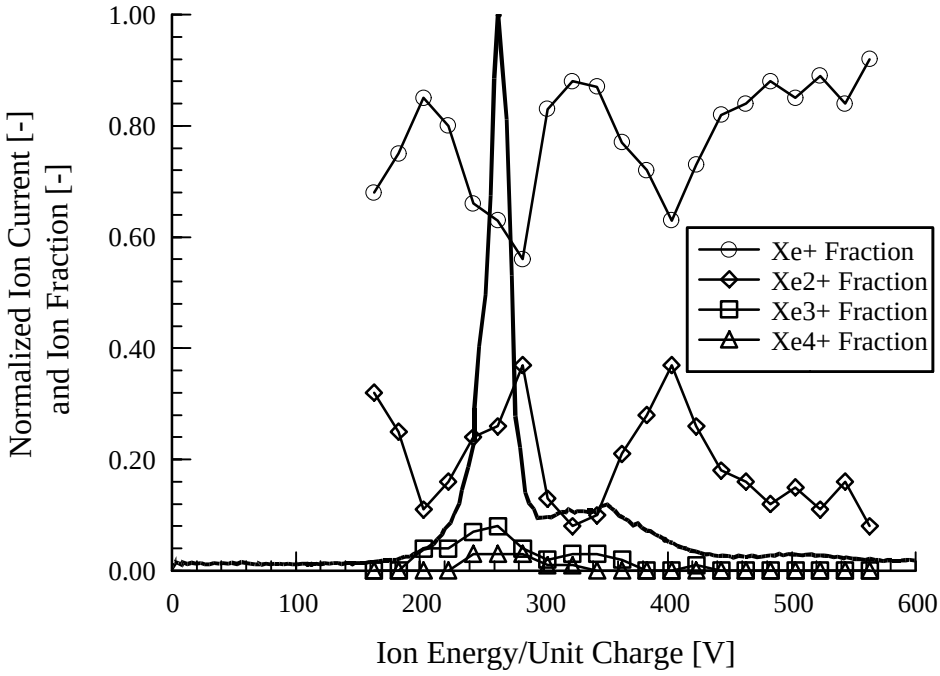

Figure 23: Near-field Ion Fractions at Condition 1 - 0 Degrees

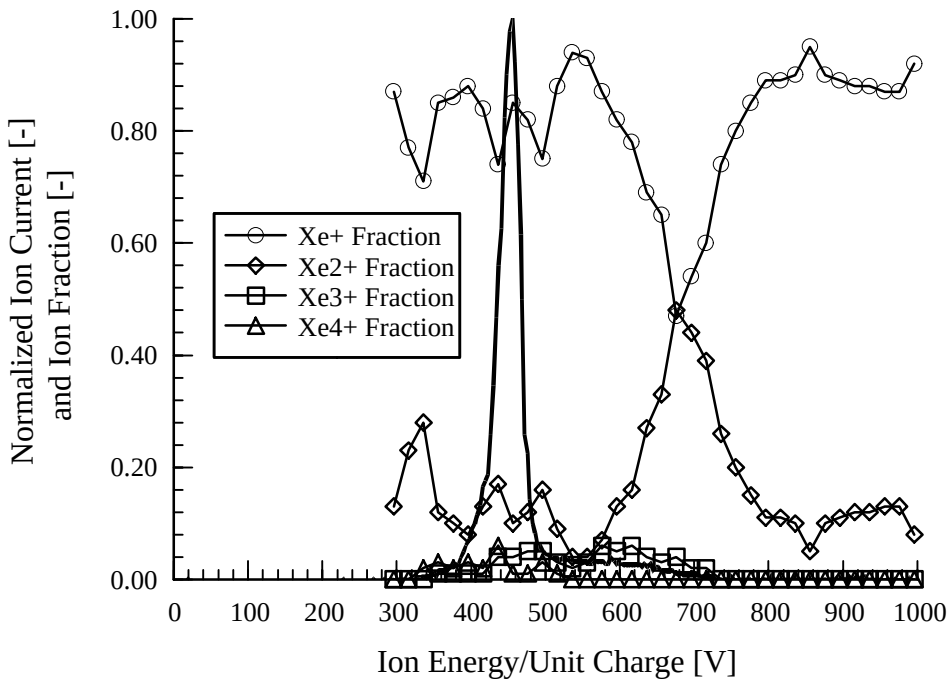

Figure 24: Near-field Ion Fractions at Condition 2 - 0 Degrees

DATA ANALYSIS

There are three primary variables examined in ion energy measurements: power, angle, and sampling location. The effects of changes in these variables will now be discussed.

Examining the changes between the thruster operating conditions, we see very similar trends between Condition 1 and Condition 2, the two cases at 5.5 A (total flow of 64 sccm). The changes in structure with angle are nearly identical. For Condition 3, at 10 A (111 sccm), the distributions are much broader in the far field. Since there is more propellant, the background pressure of neutral xenon in front of the thruster will be higher, thus increasing the amount of collisional broadening. However, the overall variation with angle is still fairly consistent with the lower discharge current conditions. The primary driving force in altering these distributions is change to the thruster's magnetic field. When the operating condition of this thruster is changed, the electromagnet coil currents are also changed. The values used for the electromagnet currents were determined during performance measurements, and were set to minimize discharge current (thus maximizing efficiency). It is presumed that altering the intensity of the magnetic field in this way also results in an alteration of the shape of the magnetic field. Thus, unlike a commercial thruster, the P5 has not undergone magnetic field optimization for the plume shape.

In presenting the changes in ion energy distribution with angle, an attempt to divide the plume into several zones was made. Of course, these zones do not have finite boundaries, and the characteristics seen in them often overlap, thus the zones are created for the purpose of clarity. The angular boundaries of these zones are different for the different operating conditions.

In the far field, the first zone is the primary discharge region near 0 degrees, as seen in Figure 7. The ions accelerated in this manner are those created by collisions with electrons trapped around radial or near-radial magnetic field lines in close proximity to the end of the discharge chamber. In other words, these are the ions that are desired in a Hall thruster, which create a majority of the useful thrust. The intensity of peaks in this zone are the highest, thus a majority of propellant ions are concentrated in this zone.

Next in the far field is a low energy region, typically extending from 40 to 70 degrees, with ions that have energy/charge ratios less than the primary peak shown in Figure 9. They do not, however, have voltages or other characteristics that correspond to CEX collisions. It is conjectured that these ions are accelerated outside of the discharge chamber, by electric field lines parallel to magnetic field lines with significantly greater curvature than those in the primary discharge region. Magnetic field lines in a Hall thruster serve essentially as lines of equipotential, with electrons being preferentially trapped by the strongest magnetic field lines – which are designed to be those radial to the Hall thruster (where the primary discharge region ions are created and accelerated). Progressing outward from the discharge chamber, the electric potential drops and the magnetic field lines obtain greater curvature. Thus, they accelerate ions at off-centerline angles with voltages significantly less than the discharge voltage (the distribution of ions accelerated near 0° from these field lines is overwhelmed in the measurements by ions from the primary discharge region). As will be explained in the near-field section, it is thought that these ions originate from the far side of the discharge chamber and are accelerated inward, across centerline. When these crossover ions encounter regions of higher plume density, we see large numbers of CEX collisions. These lead to significant broadening of the ion energy profile at high angles, which is shown in Figure 26 through 28.

The next two regions, where the profile returns to a centerline-like shape followed by a CEX region, are the most puzzling. In both these regions ions are accelerated by the same potential that the primary discharge regions ions are, but at a large angle. It is theorized that the field lines that produce the primary discharge ions are not completely linear, but instead have a sharp curvature on the inward side of the discharge chamber. Ions created in this region will be accelerated normal to the field lines, thus creating ions that experience the same accelerating potentials as centerline ions but are directed in the range of 60 to 80 degrees with respect to centerline. As the angle is increased toward 90 degrees, these ions encounter the acceleration region on the opposite side of the discharge chamber, undergoing large numbers of CEX collisions.

Beyond 90 degrees, we see a small region of low energy ions. These are created along magnetic field lines with very large radii, such that they curve beyond 90 degrees and accelerate the ions backwards with respect to the desired thrust vector. The energy of these ions is low, since they were created along a field line relatively far outside the discharge chamber.

One of the surprising results of this study was that there did not appear to be any ions at angles significantly beyond 90 degrees. King found ions at 180 degrees, directly behind the thruster.[13] However, examining the SPT-100, we note that the magnetic pole pieces are designed to minimize mass and thus are – wherever possible – narrower than the magnetic cores. The P5 was designed with extra wide pole pieces (see Figure 1) to minimize magnetic field leaking. These pole pieces act as a shield that prevents ions from flowing backward

In the near field we see, as expected, the primary discharge region near centerline (see Figure 12). Going outward in the plume, we do not see the low energy region that was seen in the near field. However, looking at the thruster orientation, we realize that with the sampling orifice centered on the annular discharge chamber (see Figure 5), ions from the far side cannot enter the orifice, except at high angles. Thus the crossover low energy ions are not seen because they do not enter the orifice. What we see instead are higher angle inwardly directed particles, those that are responsible to the return to centerline and CEX regions in the far-field as seen in Figure 9 at 75 and 85 degrees, respectively. These result in ion energy distributions like those shown in Figure 15 at 55 and 70 degrees. This behavior continues to dominate all the way out to loss of signal.

If the ion energy distributions observed at angles outside the primary discharge region were the result of ions travelling radially outward from the discharge chamber, then there should be very little variation in their shape, since at all angles the plasma would be undergoing CEX collisions with the uniform background neutral gas. However, if the ions are travelling radially inward, we expect much greater variation since the plasma would be encountering ions and neutrals from the other side of the annulus, the

density of which will increase with angle (as the beam path moves closer to the exit plane of the discharge chamber). This appears to be what was observed in this investigation. For this to be correct, however, the density must be high enough that the mean free path for ion-neutral CEX collisions is on the order of (or less than) the diameter of the discharge chamber (~ 15 cm). Measurements taken inside of a D-55 TAL[18] indicate pressures on the order of 1 mTorr for equivalent flow rates. Calculations for the P5 also indicate a neutral pressure of approximately 1 mTorr based on a neutral temperature of 1000 K and a neutral velocity of 300 m/s. At these pressures, the ion-neutral CEX collision mean free path[19] was determined to be 5 cm. Thus, the density is high enough to support this conclusion. Therefore, as a consequence of this analysis, it appears that most of the ions produced by this thruster are either accelerated axially along the thrust vector or have an inwardly directed radial component, toward thruster centerline. This conclusion is supported by Langmuir probe measurements taken inside the discharge chamber by Haas using a high speed reciprocating probe.[10] These measurements show plasma equipotential lines that curve back toward the anode in the inner portion of the discharge chamber; and ions are accelerated perpendicular to equipotential lines. There are also two other pieces of evidence to support inward acceleration. First, visual inspection of the thruster while firing shows a plume with a single central core. This differs from other thrusters, such as the SPT-100, which demonstrate a double peaked core, corresponding to the annular nature of the thruster discharge chamber. Second, as part of this research effort an attempt was made to obtain ion energy and time-of-flight measurements in the very near field, 1 cm from the exit of the discharge chamber. Measurements were made, but operating the thruster in such close proximity to an obstruction led to unacceptable interference with thruster operation with a marked increase in thruster current. Therefore, the effort was abandoned. However, the plots that were taken in 5 mm increments across the face of the discharge chamber do show a repeatable qualitative trend toward higher intensity on the inner half of the discharge chamber than on the outer. Since, to a first approximation, equipotential lines follow magnetic field lines, these facts seem to confirm that the magnetic field structure of the P5 is such that the plume is focused inward.

When we compare individual near field ion energy traces to those taken in the far field, we see a number of differences. Figure 25 shows the 0 degree ion energy profiles for Condition 1 in the near field and far field. They have been normalized and overlaid for comparative purposes.

The first thing that we notice is that the trace taken at 10 cm is significantly narrower than that taken at 75 cm. The full width at half maximum in the near field was 22 V, as compared to 35 V in the far field. The increased width appears as low energy elastic collisions. We also see that the 1.33X CEX collision observed at 10 cm has disappeared by 75 cm. In general, elastic collisions are far more prevalent in the far field than in the near field, obscuring CEX collisions in some cases. This is as expected since for ions of the energy range found in the Hall thruster,[20] CEX collisions are approximately an order of magnitude more likely than elastic collisions. Thus, by sampling close to the thruster, the plume is interrogated before it has had an opportunity to undergo a significant number of elastic collisions.

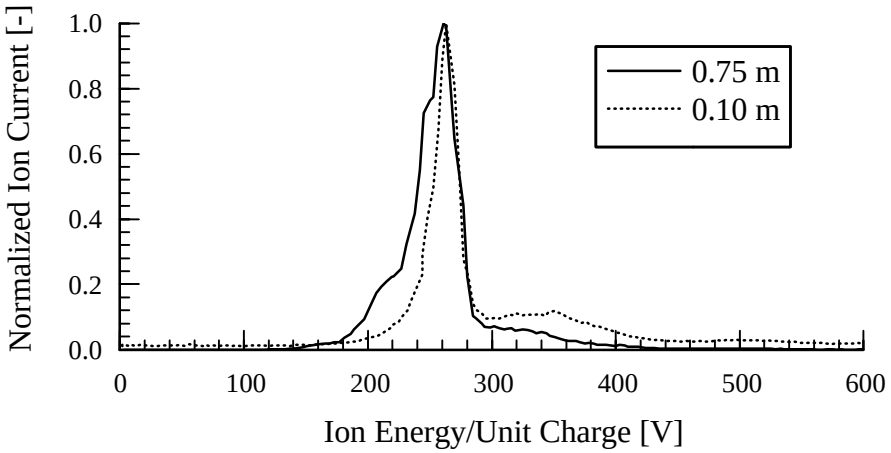

Figure 25: Normalized Ion Energy Profiles - 0 Degrees

Figures 26 through 28 show the full width at half maximum measured at near and far-field for the three conditions studied. In addition, since it is a very similar operating point, Condition 1 is compared to SPT-100 data taken by King[13] in Figure 26. The narrowing of these ion energy profiles compared to King's is a result of the improvements made to the chamber pumping capacity through the installation of cryopumps. With lower background pressure, the frequency of pressure broadening causing collisions is reduced and thus the profiles are narrower at low angles.

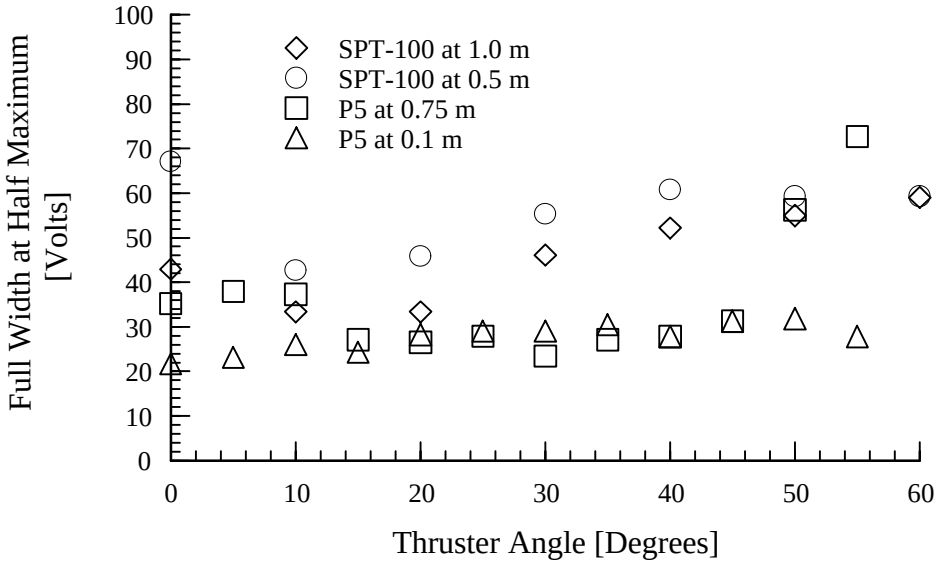

Figure 26: Full Width at Half Maximum - Condition 1 and SPT-100

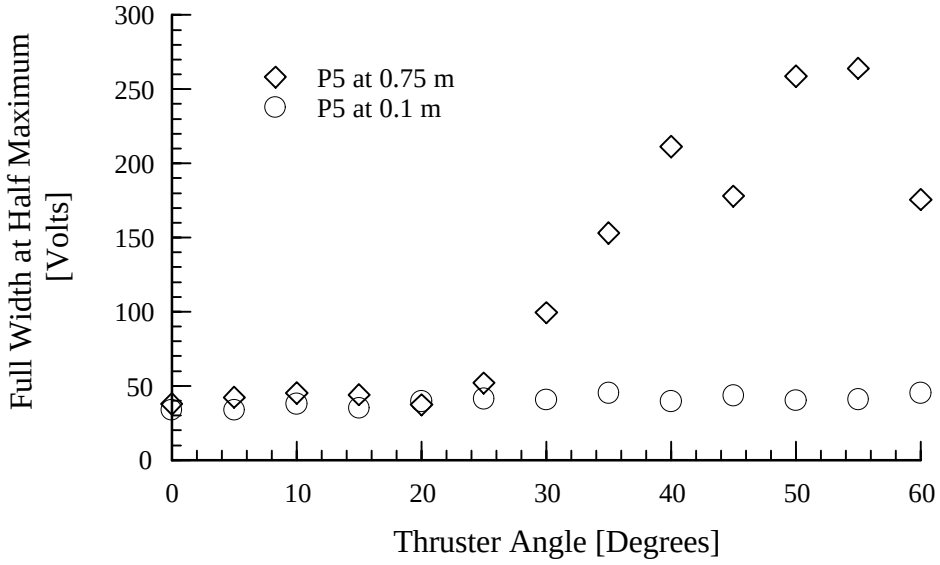

Figure 27: Full Width at Half Maximum - Condition 2

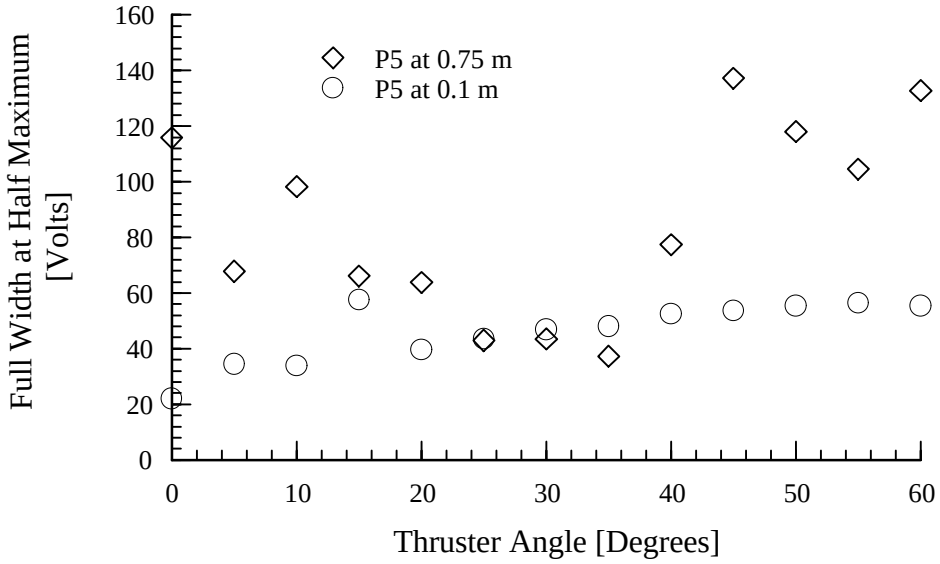

Figure 28: Full Width at Half Maximum - Condition 3

In Figure 26 through Figure 28, we see that the full width at half maximum is broadened in the far-field at low and high angles. As discussed previously, at high angles inwardly directed low energy ions crossover the centerline and collide with the flow from the other side of the discharge chamber. These collisions result in broadening of the ion energy distribution. At low angles, the conjecture was that when the thruster was firing directly toward the sampling skimmer, plasma from the thruster that does not enter the orifice impacts on the surrounding flange and is neutralized. This would represent a localized area of higher pressure neutral xenon that would cause collisions and broaden the profile. This hypothesis was checked by placing a neutral particle flux probe[21,22] just below the sampling orifice, perpendicular to the flow. The NPF grids were charged to repel all ions and electrons, and an uncalibrated ion gauge was used to obtain pressure changes relative to the background pressure measured by a calibrated ion gauge as the thruster was rotated inward. Figure 29 shows the change in pressure with thruster angle for Condition 1 and Condition 3 along with the background pressure for each condition (determined as an average of two

ion gauges and corrected for xenon). We see a notable increase in pressure within 20 degrees of centerline, the same region where the far-field full width at half maximum measurements show broadening.

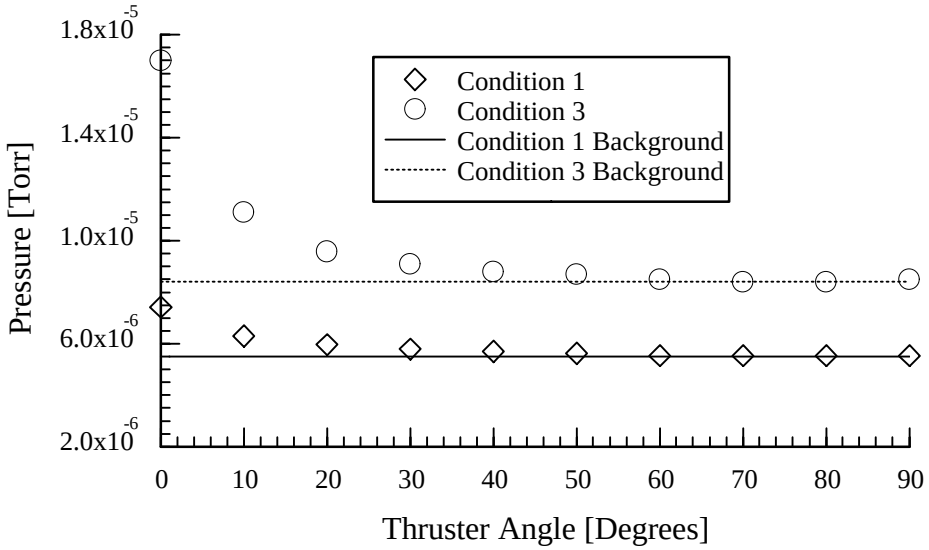

Figure 29: Pressure in Front of Far-field Sampling Orifice with Chamber Background Pressures

Therefore, based on these results, we believe that the low angle broadening in the full width at half maximum is primarily a facility effect, whereas the high angle broadening is the results of collisions caused by crossover flow.

SUMMARY

In summary, we have used ion energy diagnostics and time-of-flight mass spectroscopy to show the evidence of singly, doubly, triply, and quadruply charged xenon within the plume of the P5. We have used measurements of the ion energy distribution at various angles and axial locations to determine the ion acceleration structure of the thruster and show that the shape and magnitude of the magnetic field drive this structure, focusing the plasma inward. Finally, we have seen that sampling the plasma closer to the thruster gives a profile that has undergone fewer changes as a result of collisions within the plume and with background neutrals within the test facility.

FUTURE WORK

In order to operate the MBMS, the thruster is positioned very close to the end cap of the LVTF (see Figure 2). This configuration can lead to unacceptable levels of material sputtering, interference with thruster operation, and modification of data profiles at high thruster power levels. One approach to mitigate these problems is to use an extension to the MBMS as demonstrated in this work. This does have its limitations and can lead to material being back-sputtered onto the thruster. Another approach is to build a small version of the 45-degree parallel-plate energy analyzer that can be mounted on the interior of the chamber. Such a device, dubbed the Miniaturized Ion Energy Analyzer (MIEA), is currently under development at PEPL. The MIEA does not perform time-of-flight measurements like the MBMS, operating strictly as an energy analyzer. A full presentation on the probe and its capabilities will be presented at the International Electric Propulsion Conference in October 1999. Some preliminary information is provided below.

A schematic of the MIEA appears in Figure 30. The probe design was driven by the need to build a small, mobile instrument that could be mounted anywhere inside a vacuum chamber. In the LVTF, this will most likely be near thruster station one, as shown in Figure 2. To achieve a reduction in probe diameter the device resolution was relaxed to 1% (the MBMS has 0.4% resolution). This corresponds to 1 mm entrance slits on the plates. The main tube that houses the plates measures 210 mm long by 38 mm in diameter. Solid Teflon rings support the plates. A Swagelok fitting leads to a turbopump that evacuates the interior. For alignment purposes, a laser is passed through the entrance orifice and out a removable alignment screw and plate. An adjustment screw allows the plates to be moved if required. As with the MBMS, a K and M Electronics model 7550m channel electron multiplier is used to measure ion current. The probe is machined from stainless steel except for the Teflon support rings and a graphite shield (not shown in Figure 30) which is used to reduce sputtering and protect the probe.

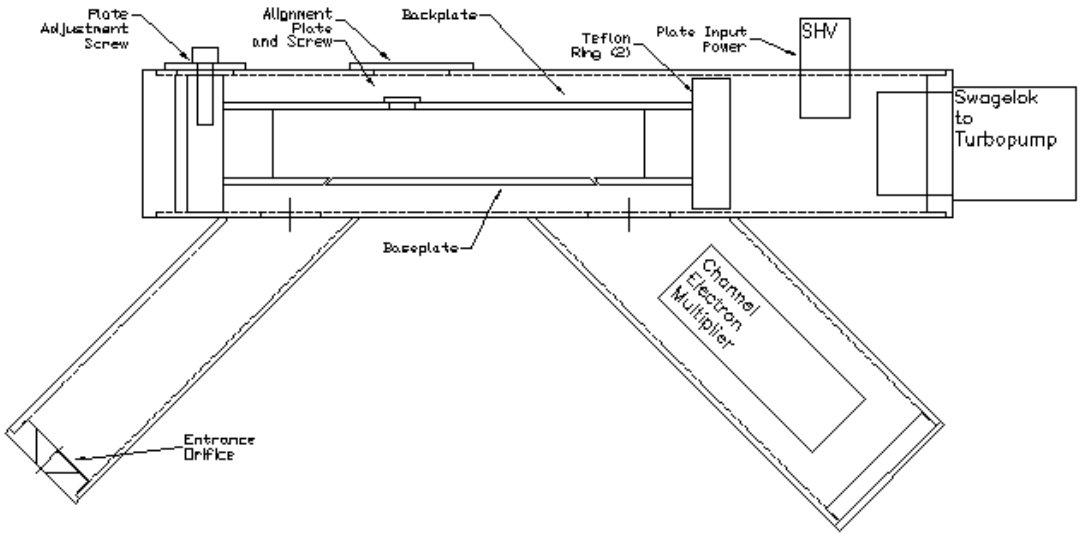

Figure 30: The Miniaturized Ion Energy Analyzer (MIEA)

Preliminary results from the probe are shown in Figure 31 for the thruster at Condition 1 on centerline, 1 m downstream of the exit plane. Ion current is normalized with the maximum recorded current in the figure. Data from the MBMS is also shown for comparison. The slit width for these tests was 2 mm, giving the device a resolution of 2.2%. The reason for this is that the 1 mm slits had not yet been manufactured via laser machining. Also, the turbopump had not yet been added. Instead, the Swagelok fitting was simply left open to the chamber. The MBMS was used to fine tune the spectrometer constant of the MIEA so that the peaks would coincide. This was done because the MIEA spectrometer constant is very sensitive to dimensional inaccuracies induced by the small size of the probe. A known source of ions will be used to formally calibrate the spectrometer constant in the immediate future. Note also that CEX collision peaks are not evident in the data collected by the MIEA. This highlights an immediate advantage of the MIEA over the MBMS. Because the MIEA is away from the vacuum chamber walls there is no pressure build-up around the thruster and the probability of an ion experiencing a CEX collision is minimized. Thus, the ion energy distributions obtained by the MIEA are thought to more accurately reflect the distribution one would encounter in the actual space environment. Finally, the FWHM for the MBMS is 29 V and the MIEA is 48 V. The addition of the turbopump should decrease this broadening which is thought to be induced by pressure build-up within the probe. These preliminary results show that the device is operating as intended and will mitigate the problems of firing the thruster into the endcap of the LVTF.

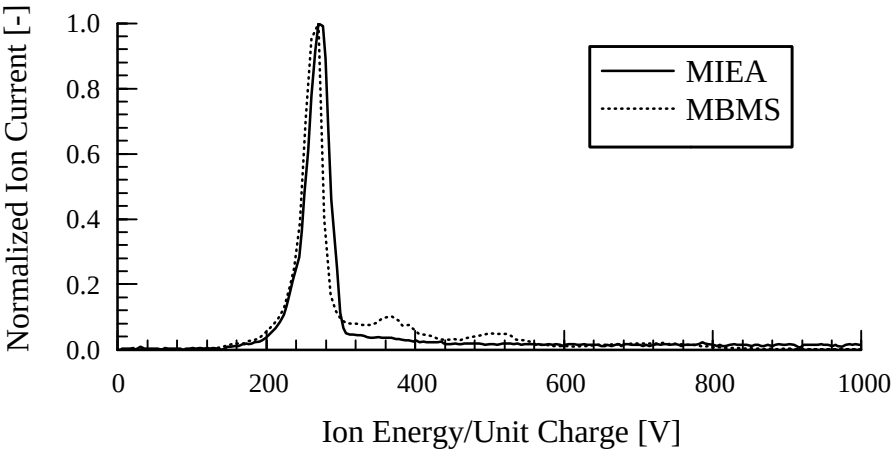

Figure 31: Initial MIEA results compared to MBMS data. Condition 1 – 0 Degrees – 1 m

ACKNOWLEDGEMENTS

The research contained herein was sponsored by the Air Force Office of Scientific Research under Dr. Mitat Birkan; this support is gratefully acknowledged. The authors would like to thank the United States Air Force Research Laboratory for their assistance in the development and construction of this thruster. They would also like to thank Mr. Michael Patterson of the NASA Glenn Research Center for the loan of the Hollow Cathode Assembly used during a portion of this study. Special thanks to their fellow researchers at PEPL for assistance during experimental setup and operations and to the technician staff of University of Michigan's Department of Aerospace Engineering. Mr. Frank Gulczinski is supported by the United States Air Force Palace Knight Program.

CONTACT INFORMATION

For further information, consult the PEPL web page at: http://www.engin.umich.edu/dept/aero/spacelab/ or contact the authors via e-mail:

- Frank Gulczinski: svhs@engin.umich.edu
- Richard Hofer: richard@hofer.com
- Alec Gallimore: alec.gallimore@umich.edu

REFERENCES

[1] Manzella, D.H., et al., "Performance Evaluation of the SPT-140," IEPC 97-059, 25th International Electric Propulsion Conference, August 1997.
[2] Sankovic, J.M., Haag, T.W., and Manzella, D.H., "Performance Evaluation of a 4.5 kW SPT Thruster," IEPC 95-030, 24th International Electric Propulsion Conference, September 1995.
[3] Tverdokhlebov, S.O., and Garkusha, V.I., "High-Voltage Mode of a TAL Thruster Operation," IEPC 97-023, 25th International Electric Propulsion Conference, August 1997.
[4] King, D., et al., "Development of the BPT Family of U.S.-Designed Hall Current Thrusters for Commercial LEO and GEO Applications," AIAA 98-3338, 34th Joint Propulsion Conference, July 1998.
[5] Haas, J.M., et al., "Performance Characteristics of a 5 kW Laboratory Hall Thruster," AIAA 98-3503, 34th Joint Propulsion Conference, July 1998.
[6] Arkhipov, B., et al., "Extending the Range of SPT Operation: Development status of 300 and 4500 W Thrusters," AIAA 96-2708, 32nd Joint Propulsion Conference, July 1996.
[7] Garner, C.E., et al., "Evaluation of a 4.5 kW D-100 Thruster with Anode Layer," AIAA 96-2967, 32nd Joint Propulsion Conference, July 1996.

[8] Petrosov, V.A., et al., "Investigation 4.5 kW High Efficiency Hall Type T-160 Electric Thruster," IEPC 95-03, 24th International Electric Propulsion Conference, September 1995.
[9] Williams, G.J., et al., "Laser Induced Fluorescence Measurement of Ion Velocities in the Plume of a Hall Effect Thruster," AIAA 99-2424, 35th Joint Propulsion Conference, June 1999.
[10] Haas, J.M., et al., "Hall Thruster Discharge Chamber Plasma Characterization Using a High Speed Reciprocating Electrostatic Probe," AIAA 99-2426, 35th Joint Propulsion Conference, June 1999.
[11] Bilen, S., et al., "Resonance-Probe Measurements of Plasma Densities in Electric-Propulsion Plumes," AIAA 99-2714, 35th Joint Propulsion Conference, June 1999.
[12] Davis, C., Gilchrist, B., and Gallimore, A.D., "Density and Spectral Measurements Using a 35 GHz Interferometry System," AIAA 99-2718, 35th Joint Propulsion Conference, June 1999.
[13] King, L.B., *Transport Property and Mass Spectral Measurements in the Plasma Exhaust Plume of a Hall-Effect Space Propulsion System*, Ph.D. Thesis, University of Michigan Department of Aerospace Engineering, University Microfilms International, 1998.
[14] Gallimore, A.D., et al., "Near and Far-Field Plume Studies of a 1 kW Arcjet," *Journal of Propulsion and Power*, January-February 1996.
[15] Dushman, S., *Scientific Foundations of Vacuum Technique*, Vol. 4, John Wiley & Sons, Inc., New York, 1958.
[16] Zhurin, V.V., Kaufman, H.R., and Robinson, R.S., "Physics of Closed Drift Thrusters," IEPC 97-191, 25th International Electric Propulsion Conference, August 1997.
[17] Manzella, D., "Stationary Plasma Thruster Plume Emissions, IEPC 93-097, 23rd International Electric Propulsion Conference, September 1997.
[18] Marrese, C.M., et al., "Analysis of Anode Layer Thruster Guard Ring Erosion," IEPC 95-196, 24th International Electric Propulsion Conference, September 1995.
[19] Rapp, D., and Francis, W., "Charge Exchange Between Gaseous Ions and Atoms," *Journal of Chemical Physics*, Vol. 37, No. 11, 1962, 2631-2645.
[20] Brown, S.C., Ed., *Basic Data of Plasma Physics*, American Institute of Physics Press, New York, 1994.
[21] King, L.B., and Gallimore, A.D., "Gridded Retarding Pressure Sensor for Neutral Particle Analysis in Flowing Plasmas," *Review of Scientific Instruments*, 68(2), February 1997.
[22] Marrese, C.M., et al., "Field Emission Array Cathodes for Electric Propulsion Systems," AIAA 98-3484, 34th Joint Propulsion Conference, July 1998.